Chapter 10. Waves and More

10.1 Relations to Chebyshev and Pseudo-Chebyshev Forms and to Fourier Series

The Gielis formula as generalization of Lamé curves and superellipses uses trigonometric functions which are transcendental. These equations can be rewritten in terms of Chebyshev polynomials [41, 46], for $x = \cos\left(\frac{m}{4}\vartheta\right)$, based on Grandi curves. The curves defined by (9.23) can then be considered as algebraic functions. They can also be used as transformations on Chebyshev polynomials and pseudo-Chebyshev functions. For $m = 1$ and $n_{1,2,3} = p$ with p an integer, this describes supercircles and superellipses, and circles or ellipses when $m = 1$ and $n_{1,2,3} = 2$:

$$\rho(x) = \frac{1}{\sqrt[n_1]{\left|\frac{1}{a}\,T_m(x)\right|^{n_2} + \left|\frac{1}{b}\,U_{m-1}(x)\right|^{n_3}}} \cdot f(x) \tag{10.1}$$

There exists also a direct connection between pseudo-Chebyshev functions and flowers. Using Gielis transformations on Grandi or Rhodonea curves, but with $\frac{m}{2}$ [44]:

$$\rho(\vartheta; a, b, n_1, n_2, n_3, n_4) = \frac{\left|\cos\left(\frac{m}{2}\vartheta\right)\right|^{n_4}}{\sqrt[n_1]{\left|\frac{1}{a}\,\cos\left(\frac{m}{2}\vartheta\right)\right|^{n_2} + \left|\frac{1}{b}\,\sin\left(\frac{m}{2}\vartheta\right)\right|^{n_3}}} \tag{10.2}$$

this generates a wide range of naturally looking flowers (see Figure 27).

Equation (10.2) with $\frac{m}{2}$ can be rewritten in terms of the recently defined pseudo-Chebyshev functions of half-integer values $k + \frac{1}{2}$ [46, 77] (see Chapter 8):

$$T_{\frac{1}{2}} = \cos\left(\frac{1}{2}\arccos(x)\right) \quad \text{and} \quad T_{k+\frac{1}{2}} = \cos\left[\left(k + \frac{1}{2}\right)\arccos(x)\right] \tag{10.3}$$

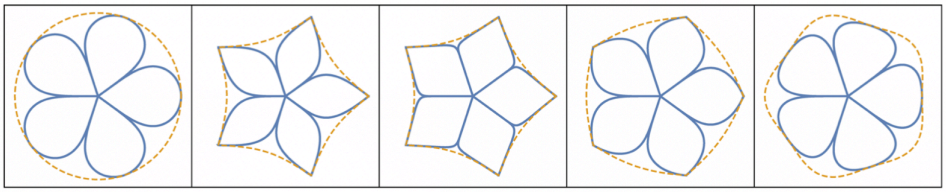

n_1	2	1	1	3	3
$n_{2,3}$	2	1	1	1	3
n_4	4	4	20	5	5

Figure 27. Choripetalous five-petalled flowers with the corresponding constraining superpolygons and parameters [44, 46].

It is remarkable that flowers and leaves are connected to these polynomials and functions. Their multiple uses in mathematics can serve as a guide in the study of botany. For the study of flowers one can make use of the orthogonality properties of pseudo-Chebyshev functions [6].

This directly leads to Fourier series solutions using pseudo-Chebyshev functions of the fourth kind. Consider for an $L_1[-\pi, \pi]$, 2π-periodic function [6]:

$$f(x) \sim \frac{1}{2}a_0 + \sum_{k=1}^{\infty} a_k \cos\left(\frac{k\pi x}{L}\right) + b_k \sin\left(\frac{k\pi x}{L}\right) \tag{10.4}$$

with a_k, b_k the Fourier coefficients of $f(x)$. By Carleson's theorem, this series converges in mean and even pointwise up to a set of Lebesgue measure zero. Since the partial sums can be written as:

$$s_n(x, f) = \frac{a_0}{2} + \sum_{k=1}^{n} a_k \cos(kx) + b_k \sin(kx) = \frac{1}{2\pi}\int_{-\pi}^{\pi} f(x-t)\, D_n(t)\, dt \tag{10.5}$$

the representation formula of the Dirichlet kernel holds:

$$D_n(\arccos(x)) = W_n(x) = 2T_{\frac{1}{2}}(x)U_{n-\frac{1}{2}}(x) \tag{10.6}$$

Here $W_n(x)$ is a pseudo-Chebyshev function of the fourth kind [6], which can be expressed using pseudo-Chebyshev functions of the first and second kind. A consequence of this result is that the partial sums of a Fourier series can be written in terms of pseudo-Chebyshev functions, as follows:

$$\begin{aligned} s_n(x,f) &= \frac{1}{\pi}\int_{-1}^{1} f(x-\arccos\tau)\; W_n(\tau)\,\frac{1}{\sqrt{1-\tau^2}}\;d\tau \\ &= \frac{2}{\pi}\int_{-1}^{1} f(x-\arccos\tau)\; T_{\frac{1}{2}}(\tau)\; U_{n-\frac{1}{2}}(\tau)\,\frac{1}{\sqrt{1-\tau^2}}\;d\tau \end{aligned} \tag{10.7}$$

The flowers in Figure 27 can be understood as a single-term Grandi curve inscribed in a polygon defined by Equation (9.23). As a generalization of Fourier series (or trigonometric series in general) each individual term of a Fourier series can be transformed. One can define a generalized series, with ρ_0, ρ_k defining a stretchable radius, as [45]:

$$\rho(\vartheta) = \rho_0 a_0 + \sum_{k=1}^{\infty} \rho_k a_k \cos(kx) + \rho_k b_k \sin(kx) \tag{10.8}$$

Since the first constant term of the series $\rho_0 a_0$ can be associated with a particular transformation ρ_0, any shape described by Equation (9.23) is described precisely in one term of this generalized series $\rho_0 a_0$ without any need for additional terms. Figure 28 shows a sum of three terms.

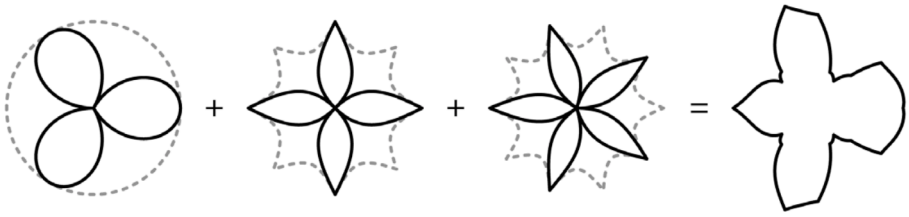

Figure 28. k-type Gielis curve with $k=3$ for $\rho(\vartheta;\, f(\vartheta),\, a,\, b,\, n_1,\, n_2,\, n_3)$. The bird is the sum of $\rho_1(\vartheta;\, \cos(\frac{3}{2}\vartheta),\, 1,\, 1,\, 3,\, 2,\, 2,\, 2)$, $\rho_1(\vartheta;\, \cos(2\vartheta),\, 1,\, 1,\, 4,\, 1,\, 1,\, 1)$ and $\rho_1(\vartheta;\, \cos(\frac{5}{2}\vartheta),\, 1,\, 1,\, 5,\, 1,\, 1,\, 1)$. [45]

10.2 Coordinate Functions of First and Higher Order and Square Waves

Equation (9.23) and the generalized Fourier series of Equation (10.8) can be used to generate waves. One example is the generation of square waves. A square wave may be generated in various ways, e.g. with reference to step functions such as the Heaviside step function (Equation 10.9). Note that the Dirac delta function is the distributional derivative of the Heaviside function [43].

$$H(x) = \begin{cases} 0 & x < 0 \\ 1 & x \geq 0 \end{cases} \tag{10.9}$$

An alternative method is synthesis via Fourier series. One well-known disadvantage of this is the Fourier-Gibbs phenomenon, whereby oscillations occur in points of measure zero. These phenomena are an inherent feature of the method, but may be mediated in practice by using $\mathrm{sinc}x = \frac{\sin \pi x}{\pi x}$ (Equation 10.10):

$$f(x) = \frac{1}{2}a_0 + \sum_{k=1}^{m-1} \mathrm{sinc}\frac{k}{m}\left[a_k \cos\left(\frac{k\pi x}{L}\right) + b_k \sin\left(\frac{k\pi x}{L}\right)\right] \tag{10.10}$$

In order to generate a square wave which is differentiable everywhere, all exponents in Equation (9.24) are equal to 1, $m = 4$ and A is very large, so that the cosine term becomes very small, ε. In Figure 29, the shape of the sine wave is given for various values of ε [43].

As long as ε is finite and not zero, the function is differentiable everywhere. In this way, Gibbs phenomena are avoided and differentiability can be ensured everywhere. These curves can also be framed in a window, e.g. the interval $[-1; 1]$ or in a Gaussian window $\frac{1}{\sigma\sqrt{2}} \exp\left[-\left(\frac{\vartheta-\mu}{2\sigma}\right)^n\right]$ for various values of ε (see Figure 30).

$$\frac{\sin \vartheta}{\varepsilon + |\sin \vartheta|} \tag{10.11}$$

Second and higher order trigonometric functions based on Equation (9.23) can be generated. Given a shape $\rho(\vartheta)$ defined by Equation (9.23),

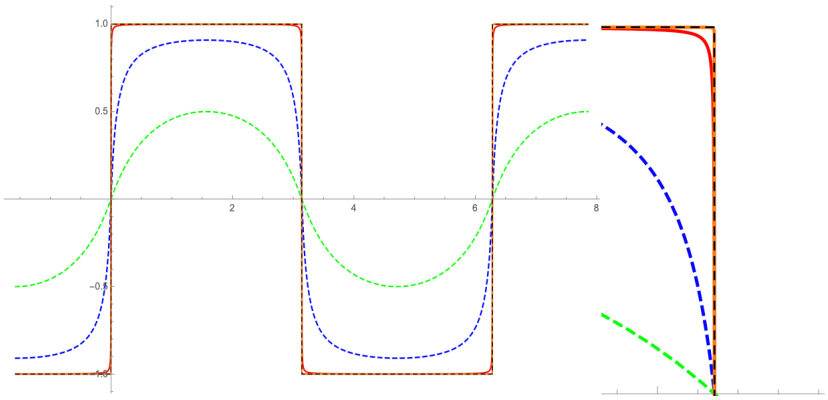

Figure 29. Sines according to Equation (10.11) for varying $\varepsilon = 10^{-\alpha}$, with $\alpha = 0$ (green), $\alpha = 1$ (blue), $\alpha = 3$ (red solid), $\alpha = 5$ (orange solid) and $\varepsilon = 0$ (black dashed) [43].

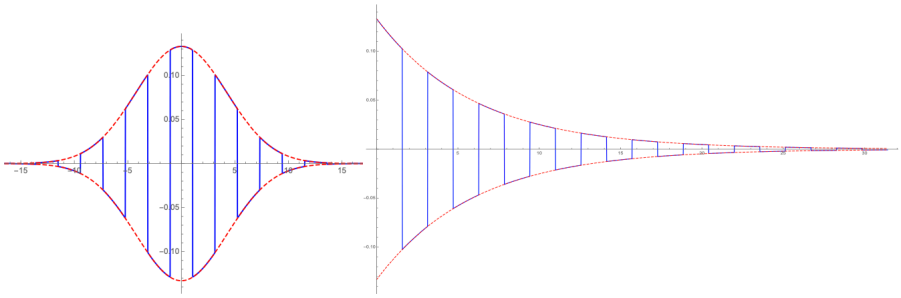

Figure 30. Left: cosines for $\varepsilon = 10^{-5}$ in Gaussian window with $n = 2$. Right: decaying square wave [43].

the polar plot is generated by:

$$\begin{aligned} c(\vartheta) &= \gamma(\vartheta)\cos(\vartheta) \\ s(\vartheta) &= \gamma(\vartheta)\sin(\vartheta) \end{aligned} \tag{10.12}$$

The functions $c(\vartheta)$ and $s(\vartheta)$ are displayed in Figure 31 with values $A = 2$, $B = 1$, $m_1 = 1.5$, $m_2 = 0.5$, $n_1 = 1$, $n_2 = 2$ and $n_3 = 3$. This can be continued to any order.

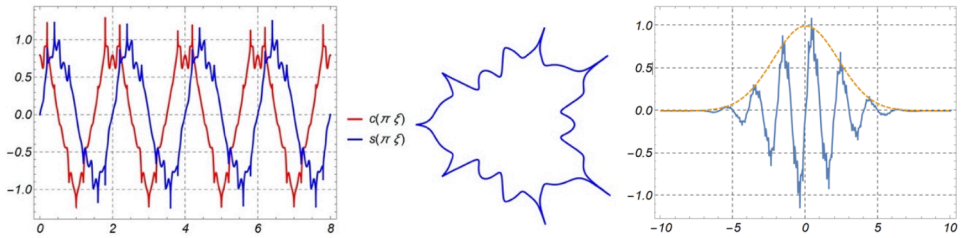

Figure 31. Supertrigonometric functions with associated polar graphs and the Gaussian version.

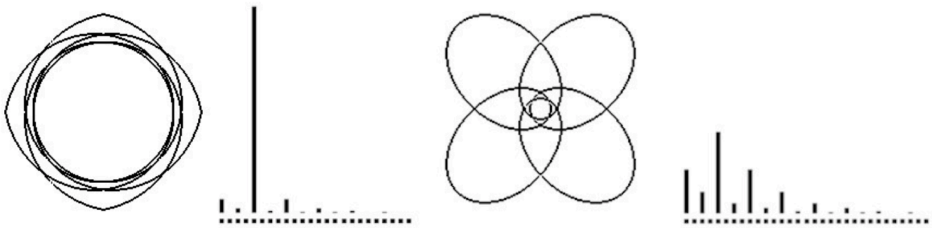

Figure 32. Polyphonic timbres inherent to Gielis curves with parameter values $\rho(\vartheta, 4/5, 1, 1, 1, 1, 1)$ (left) and $\rho(\vartheta, 4/5, 1, 1, 1, 9, 9)$ (right).

Figure 32 displays rational Gielis curves with m a rational number ($m = 4/5$). Increasing the values of the n_2, n_3 parameters lowers the magnitude of the main q-th harmonic partial (5th in this example) and raises the magnitudes of the other partials, as can be seen in the two harmonic spectra of the X-coordinates waveforms. The spectra of the Y-coordinates waveforms (not shown) have similar polyphonic spectral characteristics [27].

10.3 Higher Dimensions

Equation (9.23) can be extended to any dimension. In 3D, both spherical coordinates (Equation 10.13) [9] and parametric

representations (Equation 10.14) can be used:

$$R(\vartheta,\varphi) = c\left[\left|\frac{\sin\frac{p\vartheta}{2}\cos\frac{q\varphi}{4}}{\gamma_1}\right|^{n_1} + \left|\frac{\sin\frac{p\vartheta}{2}\sin\frac{q\varphi}{4}}{\gamma_2}\right|^{n_2} + \left|\frac{\cos\frac{p\vartheta}{2}}{\gamma_3}\right|^{n_3}\right]^{-1/n_0} \tag{10.13}$$

The parametric equation (10.14) is based on two perpendicular cross sections ρ_1, ρ_2 which can be of different sizes leading to toroidal structures (see Figures 33 & 34) [41]:

$$\begin{cases} x = \rho_1(\vartheta)\cos(\vartheta)\,\rho_2(\varphi)\cos(\varphi) \\ y = \rho_1(\vartheta)\sin(\vartheta)\,\rho_2(\varphi)\cos(\varphi) \\ z = \rho_2(\varphi)\sin(\varphi) \end{cases} \tag{10.14}$$

This can be further extended within the framework of Generalized Möbius-Listing surfaces and bodies with Equations (10.15) and (10.16) [49, 96, 97]. Both the basic line and the cross section can be defined by any of the curves discussed earlier. The lower index of the notation GML_m^n denotes the symmetry of the cross section and the upper index denotes the number of twists before joining the ends. Also classic prisms and canal surfaces belong to this class. A more general class is Generalized Rotating and Twisting bodies GRT_m^n. Examples are shown in Figures 35 and 36.

$$\begin{cases} X(\tau,\psi,\theta) = \left(R(\theta) + p(\tau,\psi)\cos\left(\frac{n\theta}{m}\right) - q(\tau,\psi)\cos\left(\frac{n\theta}{m}\right)\right)\cos(\theta) \\ Y(\tau,\psi,\theta) = \left(R(\theta) + p(\tau,\psi)\cos\left(\frac{n\theta}{m}\right) - q(\tau,\psi)\cos\left(\frac{n\theta}{m}\right)\right)\sin(\theta) \\ Z(\tau,\psi,\theta) = K(\theta) + \left(p(\tau,\psi)\sin\left(\frac{n\theta}{m}\right) + q(\tau,\psi)\cos\left(\frac{n\theta}{m}\right)\right) \end{cases} \tag{10.15}$$

or alternatively:

$$\begin{cases} X(\tau,\psi,\theta) = \left(R(\theta) + p(\tau,\psi)\cos\left(\psi + \frac{n\theta}{m}\right)\right)\cos(\theta) \\ Y(\tau,\psi,\theta) = \left(R(\theta) + p(\tau,\psi)\cos\left(\psi + \frac{n\theta}{m}\right)\right)\sin(\theta) \\ Z(\tau,\psi,\theta) = K(\theta) + p(\tau,\psi)\sin\left(\frac{n\theta}{m}\right) \end{cases} \tag{10.16}$$

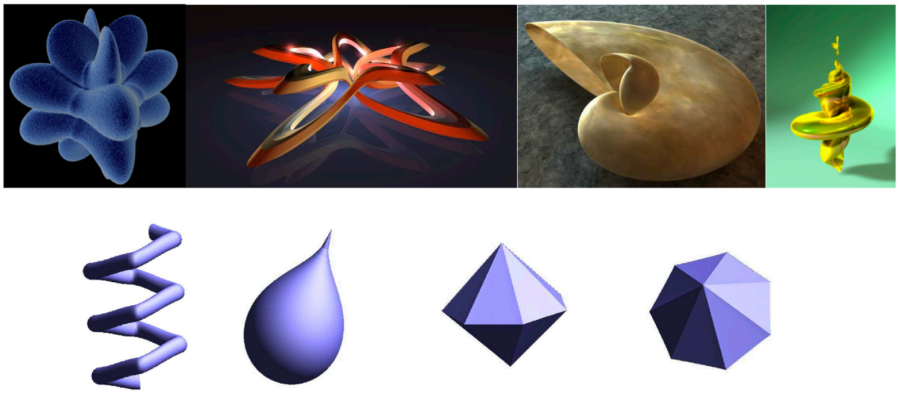

Figure 33. 3D shapes defined by Equation (10.14).

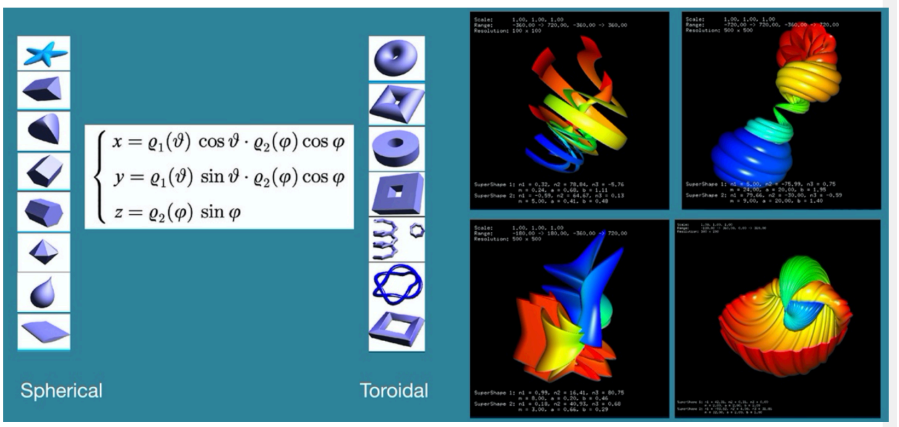

Figure 34. 3D shapes defined by Equation (10.14).

The main advantage of such general coordinate systems, as also observed by Lamé, is that to each physical shape or phenomenon a best fitting coordinate system can be found. The goal of mathematical physics then is to solve the boundary value problems associated with the problem under investigation [41, 55].

Both the cross section and the basic line can be defined by Equation (9.24) and a time component can operate on cross section, basic line and twisting parameters for dynamical studies.

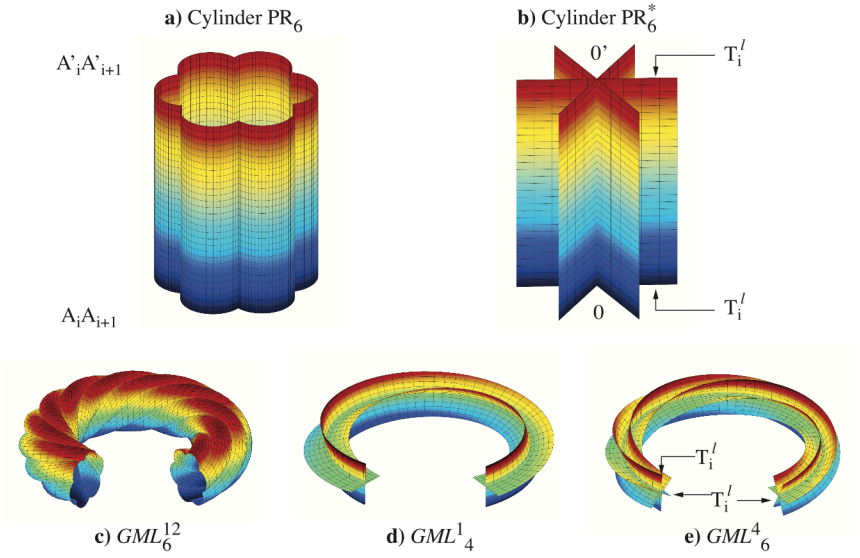

Figure 35. Prisms and GML_m^n surfaces.

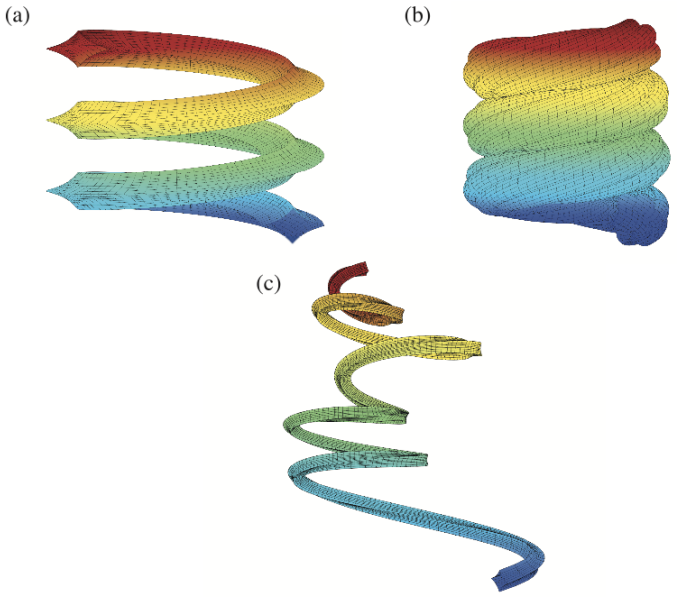

Figure 36. Generalized Rotating and Twisting bodies GRT_m^n.